J Neurophysiol 94: 2491–2503, 2005.
First published June 8, 2005; doi:10.1152/jn.00288.2005.

Visual Responses of the Human Superior Colliculus: A High-Resolution Functional Magnetic Resonance Imaging Study

Keith A. Schneider and Sabine Kastner
Department of Psychology and Center for the Study of Brain, Mind and Behavior, Princeton University, Princeton, New Jersey

Submitted 18 March 2005; accepted in final form 4 June 2005

Schneider, Keith A. and Sabine Kastner. Visual responses of the human superior colliculus: a high-resolution functional magnetic resonance imaging study. *J Neurophysiol* 94: 2491–2503, 2005. First published June 8, 2005; doi:10.1152/jn.00288.2005. The superior colliculus (SC) is a multimodal laminar structure located on the roof of the brain stem. The SC is a key structure in a distributed network of areas that mediate saccadic eye movements and shifts of attention across the visual field and has been extensively studied in nonhuman primates. In humans, it has proven difficult to study the SC with functional MRI (fMRI) because of its small size, deep location, and proximity to pulsating vascular structures. Here, we performed a series of high-resolution fMRI studies at 3 T to investigate basic visual response properties of the SC. The retinotopic organization of the SC was determined using the traveling wave method with flickering checkerboard stimuli presented at different polar angles and eccentricities. SC activations were confined to stimulation of the contralateral hemifield. Although a detailed retinotopic map was not observed, across subjects, the upper and lower visual fields were represented medially and laterally, respectively. Responses were dominantly evoked by stimuli presented along the horizontal meridian of the visual field. We also measured the sensitivity of the SC to luminance contrast, which has not been previously reported in primates. SC responses were nearly saturated by low contrast stimuli and showed only small response modulation with higher contrast stimuli, indicating high sensitivity to stimulus contrast. Responsiveness to stimulus motion in the SC was shown by robust activations evoked by moving versus static dot stimuli that could not be attributed to eye movements. The responses to contrast and motion stimuli were compared with those in the human lateral geniculate nucleus. Our results provide first insights into basic visual responses of the human SC and show the feasibility of studying subcortical structures using high-resolution fMRI.

INTRODUCTION

The superior colliculus (SC) is a laminar structure located in the midbrain that belongs to a distributed network of areas mediating saccadic eye movements, fixations, and directed attention. The SC has been extensively studied in nonhuman primates and other species using anatomical and electrophysiological techniques (for review, Krauzlis 2004b; Moschovakis et al. 1996; Sparks 1986, 2002; Wurtz and Albano 1980). The SC is subdivided into a superficial part, which mainly processes visual information, and a deeper part, which contributes to the control of orienting movements of the eyes and the head in response to sensory stimuli.

The inputs to the superficial layers of the SC include afferents from the retina (de Monasterio 1978b; Leventhal et al. 1981; Perry and Cowey 1984; Rodieck and Watanabe 1993; Schiller and Malpeli 1977), striate cortex (Finlay et al. 1976; Fries 1984; Fries and Distel 1983; Graham 1982; Wilson and Toyne 1970), extrastriate cortex (Fries 1984), and the frontal eye fields (Astruc 1971; Fries 1984; Kunzle and Akert 1977; Kunzle et al. 1976; Kuypers and Lawrence 1967). The contralateral visual field is mapped systematically in the superficial layers of each SC. The upper and lower visual field is represented medially and laterally, respectively, and the fovea and periphery of the visual field are represented anteriorly and posteriorly, respectively (Cynader and Berman 1972; Goldberg and Wurtz 1972a). Neurons in the superficial layers respond well to a broad range of transient or moving visual stimuli independent of stimulus orientation, size, shape, or movement velocity (Cynader and Berman 1972; Goldberg and Wurtz 1972a; Humphrey 1968; Marrocco and Li 1977; Schiller and Koerner 1971; Schiller and Stryker 1972). SC neurons have generally been found to be unresponsive to differences in luminance contrast (e.g., Marrocco and Li 1977), but the contrast response function has not been reported in primates. Although neurons in the superficial layers respond primarily to visual stimuli, their responses may be modulated by behavior. For example, responses evoked by a visual stimulus were found to be enhanced when the stimulus was selected as a target for an eye movement (Goldberg and Wurtz 1972b; Wurtz and Mohler 1974) or suppressed during the execution of an eye movement (Goldberg and Wurtz 1972a; Robinson and Wurtz 1976). Responses were also found to be enhanced when a monkey directed attention to a stimulus relative to a condition when the same stimulus was unattended (Robinson and Kertzman 1995).

The deeper layers of the SC receive inputs from a number of subcortical and cortical areas, but only sparse inputs from the primary sensory and motor cortices. The majority of cortical inputs arise from association areas including prefrontal cortex (Fries 1984; Goldman and Nauta 1976), the frontal eye fields (Fries 1984; Komatsu and Suzuki 1985; Kunzle and Akert 1977; Kunzle et al. 1976; Leichnetz et al. 1981; Segraves and Goldberg 1987; Sommer and Wurtz 2000), and parietal cortex (Fries 1984; Lynch et al. 1985). The deeper layers predominantly contain neurons that respond to eye and head movements, most notably immediately before a saccade is executed (Robinson and Jarvis 1974; Schiller and Koerner 1971; Schiller and Stryker 1972; Sparks 1975; Wurtz and Goldberg 1971, 1972), or to shifts of attention (Ignashchenkova et al. 2004; Kustov and Robinson 1996). Neurons in the deeper layers tend to habituate quickly and respond weakly to repeated visual

Present address and address for reprint requests and other correspondence: K. Schneider, Rochester Center for Brain Imaging, Box 278917, Univ. of Rochester, Rochester, NY 14627-8917 (E-mail: ks@rcbi.rochester.edu).

The costs of publication of this article were defrayed in part by the payment of page charges. The article must therefore be hereby marked "*advertisement*" in accordance with 18 U.S.C. Section 1734 solely to indicate this fact.

stimuli, but most do respond well to motion stimuli (Cynader and Berman 1972; Marrocco and Li 1977).

Little is known about the visual response properties of the human SC. Several studies have investigated the anatomical organization of the human SC including its cellular morphology, distribution, and laminar pattern (Hilbig et al. 1999; Laemle 1981, 1983; Leuba and Saini 1996), a possible columnar organization (Graybiel 1979; Wallace 1988), and connections between the colliculi (Tardif and Clarke 2002). These studies suggest that the SC is organized similarly in humans and other primates. The SC is difficult to study in detail with functional brain imaging techniques because of its small size, deep location, and proximity to vascular structures that cause a high degree of physiological noise in the midbrain and brain stem (Guimaraes et al. 1998; Poncelet et al. 1992). One functional MRI (fMRI) study performed at 3 T used cardiac triggering of image acquisition to reduce movement artifacts caused by blood pulsation and showed stronger activation in the midbrain evoked by stimuli presented in the contralateral hemifield compared with the ipsilateral hemifield (DuBois and Cohen 2000). Other functional imaging studies have reported activations in the human SC related to functions associated with its deeper layers, including eye and head movements (Petit and Beauchamp 2003; Schmitz et al. 2004), spatial navigation (Grön et al. 2000), visual search (Gitelman et al. 2002), and selective attention to motion (Büchel et al. 1998) or shape (Corbetta et al. 1991). Despite the growing body of knowledge about the human SC, a detailed account of its retinotopy and basic visual properties that are primarily associated with its superficial layers is missing.

Here, we used high-resolution fMRI techniques to study the retinotopic organization and basic visual properties of population responses in the SC. The midbrain was scanned with 2-mm-thick coronal slices, each with an in-plane resolution of 1.5×1.5 mm^2. In separate experiments, several visual stimuli were used, including periodic flickering checkerboard stimuli to study the retinotopic organization, checkerboards of varying luminance contrast to obtain contrast response functions, and moving and stationary dot fields to study responsiveness to motion. The motion experiments included controls during which eye movements were monitored. Activations in the SC were confined to stimuli presented in the contralateral hemifield. Further details of the topographic organization were observed in individual subjects. The SC response was highly sensitive to low stimulus contrast and stimulus motion. Our results show that high-resolution fMRI can be used effectively to study response properties of the human SC.

METHODS

Subjects

Eleven subjects participated in the study, which was approved by the Institutional Review Panel of Princeton University. All subjects (22–35 yr old, 4 males) were in good health with no history of psychiatric or neurological diseases and gave their informed written consent. Subjects had normal or corrected-to-normal visual acuity. Seven subjects (S1–S7) participated in two separate scanning sessions to measure the polar angle and eccentricity components of the retinotopic maps. Seven subjects (S1–S4, S6, S10, and S11) participated in a session to measure responses to 10 and 100% stimulus contrast; four of these subjects (S2, S6, S10, and S11) participated in a second session to measure responses to 5 and 25% contrast. Four subjects (S1, S2, S6, and S8) participated in a session to measure the response to stimulus motion. Three subjects (S6, S9, and S11) participated in a session in which their eye movements were monitored while viewing the motion stimulus. Subjects S1–S7 correspond to those reported in a related study of the human lateral geniculate nucleus (LGN) (Schneider et al. 2004).

Visual stimuli and display

Four different visual stimuli were used in this study. The first three stimuli consisted of checkerboard patterns whose components reversed contrast at 8 Hz. The full checkerboard pattern, only a portion of which was revealed at any point in time, encompassed the central 15° of the visual field (13° near the vertical meridian) and contained 24 radial sectors and 12 evenly spaced annuli (Fig. 1, *A–C*). The luminances of the alternating bright and dark sections of the checkerboard were chosen such that the mean luminance of the stimulus was the same as that of the neutral gray background (147.1 cd/m^2); the contrast (defined as the difference in luminances divided by their sum) between the checkers was 97.9% in the retinotopic mapping studies and varied in the studies probing the contrast response function as described below. In all visual displays, a central fixation point was present, and subjects were instructed to maintain fixation for the duration of each scanning run while passively viewing the stimuli.

Rotating hemifield and expanding ring stimuli (Fig. 1, *A* and *B*) were used to determine the polar angle and eccentricity components of the retinotopic maps (DeYoe et al. 1994, 1996; Engel et al. 1994, 1997; Sereno et al. 1995). The visible portion of the rotating hemifield stimulus slowly and smoothly rotated counterclockwise about the point of fixation. The expanding ring stimulus consisted of an annulus with thickness equal to one-half of the radius of the visual display that expanded from the fixation point. The annulus increased in eccentricity (i.e., the distance from fixation) and wrapped around to the center once it reached the outer edge of the display. For two subjects (S6 and S7), the ring stimulus was reversed, contracting rather than expanding. Both the hemifield and ring stimuli swept through the visual field with a period of 32 s, thereby evoking waves of activation in neurons through whose receptive fields they passed. Each region of the stimulated visual field was exposed to a flickering checkerboard pattern during one-half of the stimulus period and the neutral gray background during the other half. The stimulus waveform was thus a square wave whose temporal phase varied depending on the position within the visual field; the positional representation of an activated voxel could be inferred from the temporal phase of its evoked hemodynamic response.

An alternating hemifield stimulus (Fig. 1*C*) was used to measure four points (5, 10, 25, and 100%) of the contrast response function. This stimulus consisted of a flickering checkerboard pattern covering one hemifield but sparing the vertical meridian and central 1.1° of the visual field. The pattern alternated between the left and right hemifields every 16 s. In separate scanning runs, the stimulus was presented at 5, 10, 25, or 100% contrast.

A fourth stimulus was used to study responses evoked by stimulus motion. The display consisted of a black background on which 2,000 small (0.1° diam) white dots were presented filling the central 15° of the visual field but sparing the central 1°. During the first 16 s of each stimulus cycle, the dots moved radially at 7°/s, one-half toward and one-half away from the fixation point. When a dot reached the center or edge of the annulus, it would reappear at a random location along the edge or center. During the second 16 s of each cycle, the dots remained stationary. Because of the temporal characteristics of the LCD projector, the luminance of the moving dot field was less than that of the static field, 105 versus 55 cd/m^2 near the fixation point, although stimulus contrast remained nearly 100% in each case. Eye movements were recorded during several sessions with this stimulus type. During eye tracking, the stimuli were projected through a neutral

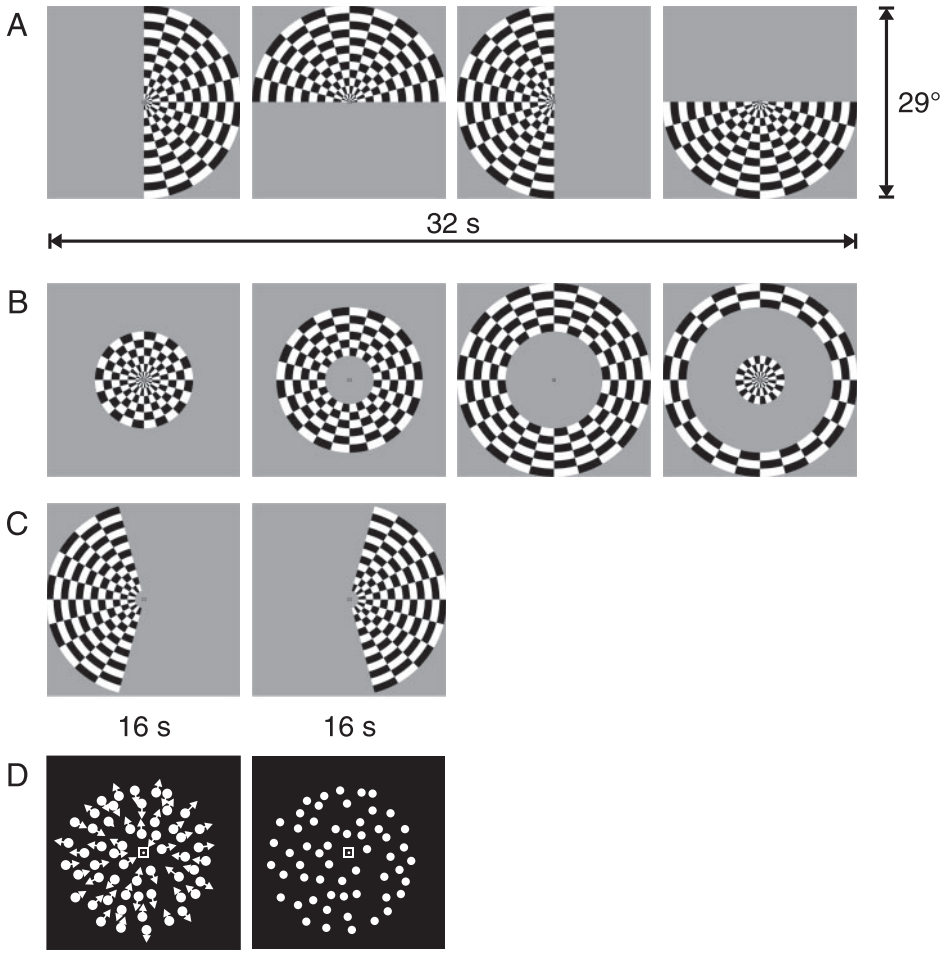

FIG. 1. Visual stimuli. Stimuli in *A–C* were contrast-reversing (8 Hz) checkerboard patterns. *A*: hemifield pattern, smoothly rotating counterclockwise, was used to map the polar angle representation. *B*: expanding or contracting ring pattern was used to map representation of eccentricity. Four frames during the 32-s period are shown for stimuli in *A* and *B*. *C*: hemifield pattern that alternated every 16 s between the left and right hemifields was used to measure responses to stimulus contrast. In separate runs, stimulus was presented at either 10 or 100% luminance contrast. *D*: motion stimulus consisted of a black background on which 2,000 small (0.1°) white dots were presented that filled an annulus from 1 to 15° from the fixation point. For the 1st 16 s of each cycle, dots moved radially, half inward and half outward, at 7°/s. For the 2nd 16 s of each cycle, dots were stationary.

density filter, which lowered the luminances of the static and moving dot fields to 9.5 and 5.0 cd/m^2, respectively, but the contrast of the dots remained high.

The stimuli were generated on a Macintosh G4 computer (Apple Computer, Cupertino, CA) using Matlab software (The Mathworks, Natick, MA) and Psychophysics Toolbox functions (Brainard 1997; Pelli 1997) and were projected from a PowerLite 7250 LCD projector (Epson, Long Beach, CA) outside the scanner room onto a translucent screen located at the end of the scanner bore. Subjects viewed the screen at a total path length of 60 cm through a mirror attached to the head coil. The screen subtended 30° of visual angle in the horizontal dimension and 26° in the vertical dimension. Luminances were measured with a Minolta CS-100 or LS-100 photometer (Konica Minolta Photo Imaging USA, Mahwah, NJ). A trigger pulse from the scanner synchronized the start of the stimulus presentation to the beginning of the image acquisition.

Data acquisition

Data were acquired with a 3 T Allegra head-dedicated MRI scanner (Siemens, Erlangen, Germany) using a standard birdcage head coil. Six to 14 series of 128 volumes each were acquired with 18 interleaved coronal slices (thickness = 2 mm with no gap between slices, except for subjects S5 and S7 who were scanned using a 1-mm gap during the polar angle session) and a gradient echo, echo planar sequence with a 128 × 128 matrix leading to an in-plane resolution of 1.5 × 1.5 mm^2 (TR = 2 s, TE = 41 ms, flip angle = 90°). A partial Fourier factor of 7/8 was used to acquire an asymmetric fraction of k-space to reduce the acquisition time. The posterior edge of the acquisition volume was aligned in the midsagittal plane with the posterior edge of the corpus callosum to cover the posterior thalamus and midbrain. Echo-planar images were compared with a coaligned high-resolution anatomical scan of the same subject's brain taken at the beginning of the session (FLASH, TR = 150 ms, TE = 4.6 ms, flip angle = 90°, 256 × 256 matrix, 6 averages) and a high-resolution anatomical volume acquired in a separate session (MPRAGE sequence; TR = 2.5 s; TE = 4.38 ms; flip angle = 8°; 256 × 256 matrix; 1-mm^3 resolution). The subjects' heads were surrounded by foam to reduce head movements; one subject (S2) also used a bite bar.

Six different types of scanning sessions were performed, in each of which identical stimuli were repeated during multiple scanning runs. In the first session, 6 (in subjects S1, S2, S5, and S7) or 12 (in subjects S3, S4, and S6) runs were acquired during the presentation of the rotating hemifield stimulus. In the second session, 12 runs were acquired for the expanding ring stimulus. In the third session, eight runs of the 10% contrast alternating hemifield stimulus were interleaved with six runs of the 100% contrast stimulus. In the fourth session, eight runs of the 5% contrast stimulus were interleaved with six runs of the 25% contrast stimulus. In the fifth session, eight runs of the moving versus static dot field stimulus were interleaved with six runs of the 100% contrast alternating hemifield stimulus. In the sixth session, eye movements were recorded during six runs of the moving versus static dot field stimulus.

Data analysis

To compensate for subject head movement and scanner drift, each volume of the acquired time series was registered (Woods et al. 1998) to the fifth volume obtained during each session. For four subjects who participated in two sessions to measure the responses to four

different contrast levels (5, 10, 25, and 100%), the volumes from both sessions were registered (Jenkinson et al. 2002) to the first volume acquired in the first session to compare regions of interest (ROIs) across sessions. For each voxel in the volume, the linear trend in the fMRI time series was subtracted to remove any slow signal drift, typical in fMRI signals, and the time series was divided by its mean intensity, converting the data from the arbitrary intensity scale from the MRI scanner to units of percent signal change. The time series of each voxel were averaged across repeated scanning runs of the identical stimulus condition. The images obtained during the first cycle of visual stimulation (32 s) were discarded to avoid transient effects of signal saturation and to allow the hemodynamics to reach steady state. Therefore the time series of each voxel contained 112 time-points representing seven cycles of visual stimulation.

A Fourier analysis was performed to identify voxels activated by the stimulus (Bandettini et al. 1993; Engel et al. 1997). For each voxel, the amplitude and phase of the harmonic at the stimulus frequency were determined by a Fourier transform of its mean time series. The amplitude corresponds to the mean to peak amplitude of the best fitting sinusoid, and the phase corresponds to the temporal delay of the peak response relative to the stimulus onset. The correlation coefficient r between the harmonic and the time series was computed as the amplitude of the harmonic component divided by the square root of the time series power.

Statistical maps were thresholded at $r \geq 0.25$, corresponding to an uncorrected $P < 0.0038$. ROIs for each SC were identified as contiguous clusters of activated voxels in the anatomical location of the SC, as determined from registered high-resolution structural images of each subject. Care was taken to include in the ROIs only voxels that were clearly located in the midbrain and to exclude activations related to veins that typically exhibited a phase inversion relative to the visual stimulation. The ROI for the contrast response function contained voxels whose mean time series averaged over all four contrasts were significantly correlated with the stimulus frequency, $r \geq 0.25$.

For the purposes of comparison (but not quantitative analysis), the eccentricity images displayed in Fig. 2 were anatomically registered (Jenkinson et al. 2002) for each subject to the polar angle images. To report the Talairach coordinates (Talairach and Tournoux 1988), the statistical maps and structural images for each subject were transformed into Talairach space using BrainVoyager software (Brain Innovation, Maastricht, The Netherlands).

For the periodic retinotopic stimuli, the response phases were corrected by subtracting each subject's individual hemodynamic lag to correctly match the phase delay of the hemodynamic response of each voxel to the phase of the stimulus, and thereby localize the region of the visual field to which the neurons in the voxel responded best. The mean delay of the periodic hemodynamic response relative to the stimulus waveform for the 100% contrast alternating hemifield stimulus was 2.31 ± 0.31 s (subjects S1–S4 and S6).

Quantitative analysis of the retinotopic organization was performed using the five subjects (S1–S4 and S6) who were scanned using no gap between slices. To compute volumetric variation as a function of polar angle, the visual field was divided into 16 22.5° sectors, centered at 0 (right horizontal meridian), 22.5, 45, 67.5, 90 (upper vertical meridian), 112.5, 135, 157.5, 180 (left vertical meridian), 202.5, 225, 247.5, 270 (lower vertical meridian), 292.5, 315, and 337.5°. SC voxels from each subject were sorted into these bins based on the phase of their responses. The bins centered on the upper and lower vertical meridians contained voxels from both the left and right SC. The volume of voxels within each sector were totaled and averaged across subjects, and the mean polar angle representation was calculated as the volume in each sector divided by the area of the sector.

Average signals of fMRI time series were computed by averaging the time series over voxels within each ROI in each subject and then across subjects. For the individual response cycles presented for the contrast data, the time series were additionally averaged over the cycles within each scanning run. For display, the time series were smoothed using a five-point moving average.

Eye movement recordings

During the sessions in which eye movements were monitored, a stimulus screen was used with a 1.9°-diam hole at one edge through which the subjects' eyes were viewed through a telephoto lens (Model 504 with Long Range Optics, Applied Science Laboratories, Bedford, MA). Eye position and pupil diameter were measured at a sampling rate of 60 Hz and were recorded on the stimulus computer through a serial interface with the eyetracker control module. The eye tracking system had a resolution of 0.14°, and the manufacturer reports that it is possible to distinguish differences in relative eye position of ~0.25°.

The eyetracking data were processed to automatically detect and remove blinks. The mean gaze position during the entire scanning run, corresponding to the center of fixation, was subtracted, and the mean position, gaze speed, and pupil diameter were calculated for the data points sampled during the moving and stationary stimulus blocks. The mean gaze speed—the magnitude of the rate of change of the gaze position—during each block was computed as the length of the gaze position trajectory divided by the time duration of each block.

RESULTS

Responses to stimulus contrast

Activation maps evoked by the 100% contrast flickering checkerboard stimulus, presented in alternation to the right and left visual hemifield, are shown for three subjects in Fig. 2*A*. The top of the midbrain, the anatomical boundary of the SC, is indicated by the white dotted outlines on all activation maps depicted in Fig. 2. Detailed and magnified views of four consecutive slices through the midbrain (see boxes in central panel) with overlaid functional activity are shown. SC activations evoked by the 100% contrast alternating hemifield stimulus were centered at mean Talairach coordinates of –6, –28, –2 for the left SC and 6, –28, 1 for the right SC averaged across four subjects (SE = 1 for all coordinates). These coordinates and volumes are similar to those previously reported (Petit and Beauchamp 2003). ROIs containing each SC were defined based on functional activation and anatomy (see METHODS). The mean volume of each SC evoked by the 100% contrast checkerboard stimulus was 86 ± 14 (SE) mm^3.

The contrast response function of the SC was measured using alternating hemifield flickering checkerboard stimuli with 5, 10, 25, or 100% contrast. ROIs were defined based on voxels whose mean time series over all contrast levels was significantly correlated with the stimulus frequency. For each contrast level, time series of fMRI signals were averaged over all voxels within the ROI, across subjects, scanning runs, and cycles within individual runs to produce a mean response cycle (Fig. 3*A* for the left SC). For comparison purposes, the mean cyclic response is shown for the left LGN in Fig. 3*B*. The mean response amplitudes across subjects are plotted as a function of contrast for the SC and LGN in Fig. 3*C*. The right SC for one subject was corrupted by an imaging artifact in one session and was omitted from the analysis. The SC exhibited a relatively shallow response function with only moderate AM for increasing contrast. In comparison, the LGN response function rose more steeply at high contrast.

To study the homogeneity of the contrast response within the SC, activations evoked by the 10% contrast alternating hemi-

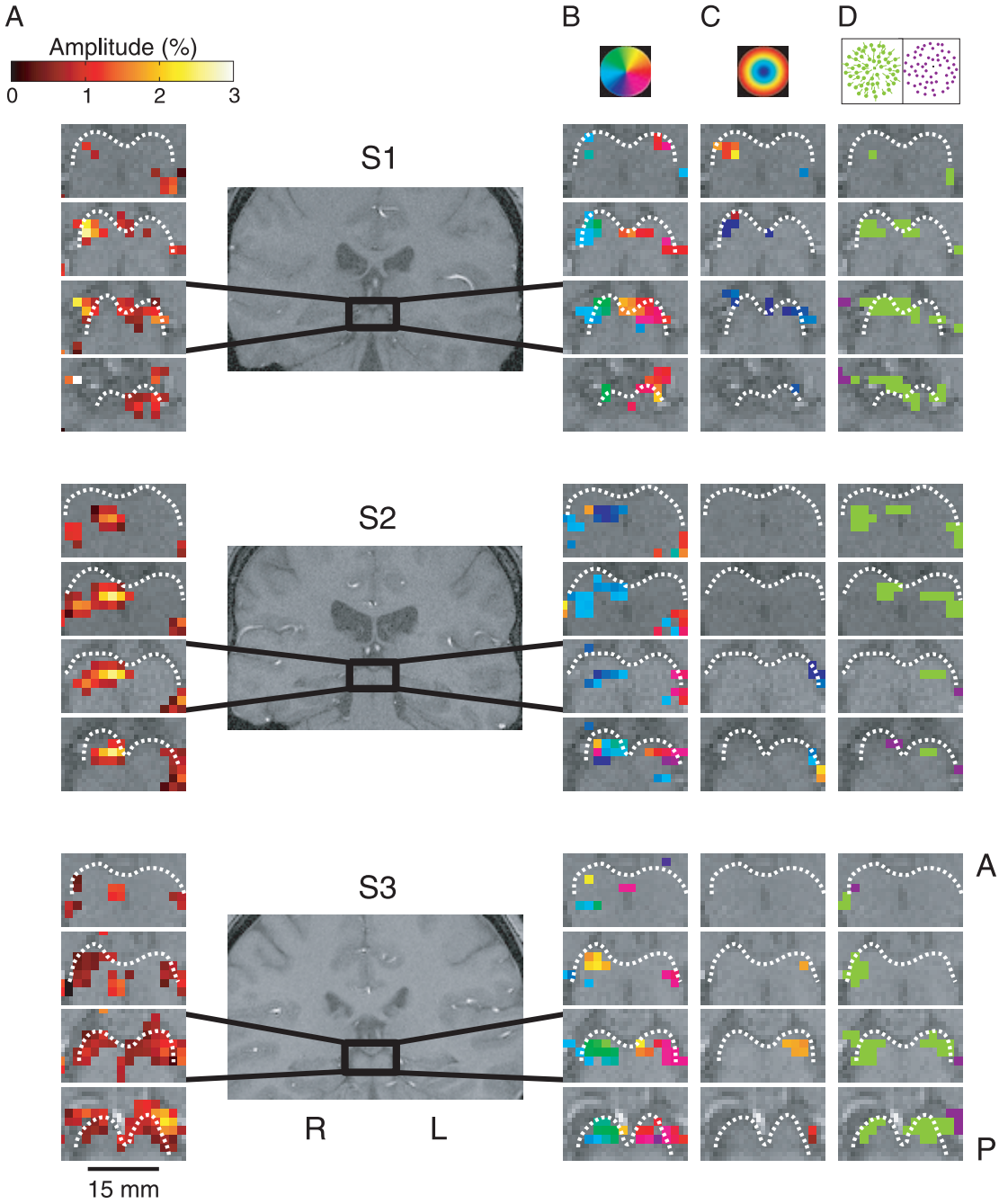

FIG. 2. Activation maps. Central panel shows an anatomical image in the coronal plane through the posterior midbrain for 3 representative subjects (S1–S3). Boxes indicate the locations of the panels to the *left* and *right*. A column of magnified regions within 4 sequential slices, arranged anterior (A) to posterior (P), is shown for each subject and each stimulus. In each of the magnified panels, a color code is given to each voxel whose response was correlated with the fundamental frequency of the stimulus, $r \geq 0.25$. *A*: responses evoked by the 100% alternating hemifield stimulus. Color code, defined at the *top* of columns, represents response amplitude of each voxel to each stimulus contrast. White dotted outlines mark anatomical boundaries of the superior colliculus (SC). *B*: representation of polar angle measured using the rotating hemifield stimulus. *C*: representation of eccentricity measured using the expanding ring stimulus. Color code indicates phase of response and labels the region of the visual field to which voxels are most responsive, as depicted in the visual field color legend at the *top* of each column. *D*: responses to moving vs. static dots. Voxels colored in green responded more strongly to moving dots, and voxels colored in purple responded more strongly to static dots.

field stimulus were compared with those evoked by the 100% contrast stimulus for each voxel that was significantly activated by both stimuli (Fig. 4*A*). The 10% contrast stimulus evoked significant activations in 63.3% (121 of 191) of voxels activated by the 100% contrast stimulus. Although the response amplitude of individual voxels varied considerably throughout the SC, a strong correlation was evident ($r = 0.89$), such that for each voxel, the larger the amplitude evoked by the 100% contrast stimulus, the larger the amplitude tended to be evoked by the 10% contrast stimulus. The linear regression line had a slope of 0.71. To further quantify the response modulation, a contrast modulation index (CMI) was calculated for each voxel, defined as $(A_{100\%} - A_{10\%})/(A_{100\%} + A_{10\%})$, where $A_{100\%}$ and $A_{10\%}$ are the mean response amplitudes evoked by

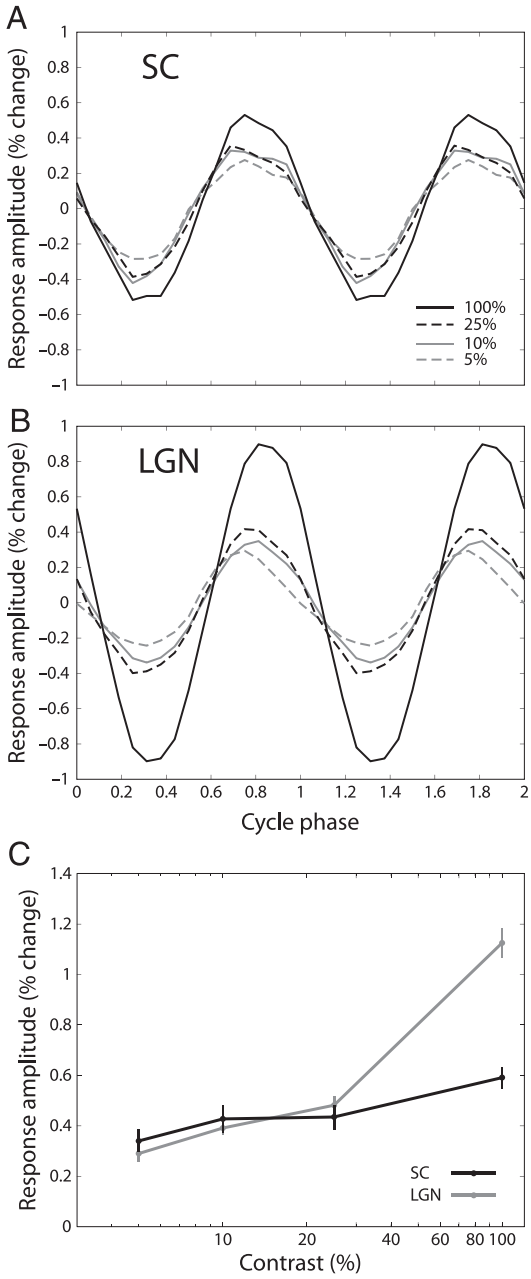

FIG. 3. Contrast responses for SC and lateral geniculate nucleus (LGN). *A*: mean functional MRI (fMRI) responses evoked by alternating hemifield flickering checkerboard stimuli with luminance contrasts of 5, 10, 25, or 100% are shown for the left SC. Mean cyclic response is shown repeated twice, averaged across voxels in the region of interest (ROI), subjects, scanning runs, and cycles within each run. *B*: mean response of the left LGN is shown for comparison. *C*: fMRI response amplitudes are plotted against contrast for the SC and LGN. Error bars depict SE.

the 100% and 10% contrast stimuli, respectively. Voxels with CMI values near 0 were weakly modulated by the increase from 10 to 100% stimulus contrast; voxels with CMI near 1 were strongly modulated. The distribution of the CMIs is shown in Fig. 4*B*. The SC contains a relatively homogenous population of voxels that are weakly modulated by stimulus contrast.

For comparison purposes, we replotted the contrast modulation data for the LGN from Schneider et al. (2004) in Fig. 4*C* and *D*. The linear regression line in the LGN had a slope of 0.22. Compared with the SC, the distribution of contrast responses among the LGN voxels was more heterogeneous, containing, in addition to the population of voxels clustered around the unity slope line that was similar to the population with small CMIs found in the SC, a more extensive population with larger CMIs (Fig. 4*C*). This secondary population of LGN voxels exhibiting a greater dynamic range for contrast response was not found in the SC and may reflect the parvocellular subdivision of the LGN.

Retinotopy

Rotating hemifield and expanding or contracting ring stimuli that traveled periodically through the visual field were used to measure the representation of polar angle and eccentricity. The rotating hemifield stimulus activated partly overlapping regions of the midbrain compared with the alternating hemifield stimuli (Fig. 2*B*). The mean volume of each SC activated by the rotating hemifield stimulus was 67.8 ± 7.2 mm^3. These activations were confined to stimulation of the contralateral hemifield. Stimulation of the right hemifield activated the left SC (Fig. 2*B,* yellow-red voxels), whereas stimulation of the left hemifield activated the right SC (Fig. 2*B,* blue-green voxels).

The polar angle representation of the SC was computed from the mean SC volume representing a square degree of visual angle within each of 16 separate sectors of the visual field, as shown in Fig. 5*A*. This analysis revealed that SC voxels generally represented locations in the visual field near the contralateral horizontal meridian; no ipsilateral activity was observed. Portions of the visual field within 30° of the vertical meridian were notably underrepresented.

In four of the seven subjects (6 of 14 SC), such as those shown in Fig. 2, a systematic topographic progression was evident such that upper visual field (green in the right SC and yellow-orange in the left SC) was represented medially and the lower visual field (blue in the right SC and purple in the left SC) was represented laterally. To quantify this organization across subjects, the distance of each activated voxel from the midline of the midbrain (measured from the cerebral aqueduct) was plotted against the elevation of its representation within the visual field (Fig. 5*B*). The activated voxels were grouped across subjects for each distance from the midline and their visual field elevations were averaged. At lateral positions 7.5 mm to the right and 6, 7.5, and 9 mm to the left of the midline, the mean elevation was significantly less than zero ($P < 0.05$, 1-tailed *t*-test); these voxels tended to represent positions in the lower visual hemifield across subjects. At the medial positions of 3, 1.5, and 0 mm to the right of the midline, the mean elevation was significantly greater than zero ($P < 0.05$); these voxels tended to represent locations in the upper visual hemifield. The mean elevation represented by voxels in intermediate positions did not differ significantly from zero; these voxels tended to represent the horizontal meridian. The topographic progression in the representation of the upper to lower visual hemifield was clearly evident across subjects from medial to lateral locations in the SC.

The SC was less well activated by the expanding ring stimulus (Fig. 2*C*), with a mean activated volume of 36.1 ± 9.1 mm^3 for each SC. This activation was mostly foveal, with an anterior to posterior progression with increasing eccentricity only apparent for two subjects (2 of 14 SC).

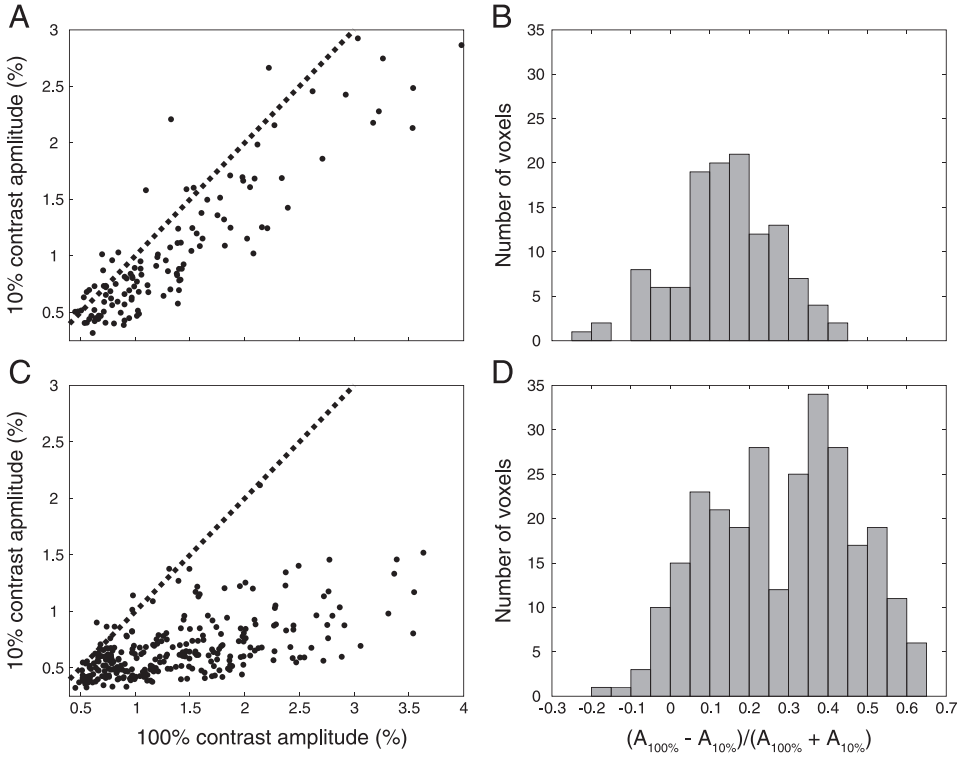

FIG. 4. Contrast modulation of individual voxels. *A* and *B*: human SC. *C* and *D*: human LGN. *A*: for each subject and each voxel activated by both 10 and 100% contrast stimuli ($r \geq 0.25$), amplitudes of the mean fMRI time series evoked by the 10 ($A_{10\%}$) and 100% ($A_{100\%}$) contrast stimuli are plotted against each other. Dotted line indicates equality between the amplitudes. *B*: distribution of the contrast modulation index (CMI) $\equiv (A_{100\%} - A_{10\%})/(A_{100\%} + A_{10\%})$. Voxels exhibiting a strong differential response to 10 and 100% contrast stimuli will have a CMI near 1, whereas those exhibiting only small response differences have a CMI near 0. Distribution shows that the majority of voxels activated in the SC region exhibited small modulations between 10 and 100% contrast stimuli. *C* and *D*: for comparison purposes, human LGN data are replotted from Schneider et al. (2004) in the same format. Unlike the SC, the LGN contains a substantial population of voxels whose responses were strongly modulated by stimulus contrast.

Responses to motion

The responses of the SC to stimulus motion were examined using a moving versus static dot display (Fig. 1*D*). Because of the full field stimulation, the division between the left and right SC could not be functionally distinguished in this paradigm, and an ROI was chosen that included both SC. The total volume activated by the motion stimulus was 263 ± 57 mm^3. Activations from three subjects are shown in Fig. 2*D*. The voxels that were activated and more responsive to the moving dots than the static dots are colored in green, whereas the few activated voxels that were more responsive to the static dots are colored in purple. The mean amplitude evoked by the motion stimulus across activated voxels and subjects was 0.76 ± 0.08% ($n = 4$). The time series of fMRI signals (Fig. 6*A*) increased during the motion phase of the stimulus (shaded epochs) relative to the interleaved epochs of stationary dot presentations. To compare the strength of the SC responses to motion stimuli to that evoked by high contrast checkerboard stimuli, an alternating hemifield stimulus (Fig. 1*C*) was also presented to the subjects in the same scanning session. This stimulus activated a total SC volume of 189 ± 46 mm^3 and evoked a mean amplitude across each SC of 0.96 ± 0.09% ($n = 8$), similar to our previous findings with this stimulus.

The flickering checkerboard stimulus activated a smaller volume than did the motion stimulus, but it also excluded a portion of the visual field along the vertical meridian, and therefore the efficiency of the two stimuli cannot be compared through a volumetric analysis. Instead, we examined the response amplitudes among the voxels activated by both the motion and the flickering checkerboard stimuli. The volume of these voxels across subjects was 144 ± 33 mm^3. The mean response amplitude over these voxels in each SC ($n = 8$) was 1.06 ± 0.12% for the flickering checkerboard stimulus and 0.82 ± 0.08% for the motion stimulus. These amplitudes were significantly different (2-tailed paired *t*-test, $t_7 = 4.46$, $P = 0.0029$). The amplitudes evoked by the motion and flickering checkerboard stimuli are plotted against each other for each individual voxel in the SC in Fig. 6*B*. The slope of the linear regression line was 0.71.

For comparison purposes, motion responses were also studied in the LGN. Across subjects, the motion stimulus activated a mean total LGN volume (including both left and right LGN) of 253 ± 40 mm^3 with a mean response amplitude of 0.69 ± 0.06% (Fig. 3*B*), compared with the 639 ± 71 mm^3 mean total volume activated by the flickering checkerboard stimulus with a mean response amplitude of 1.09 ± 0.04%. The mean total LGN volume jointly activated by both stimuli was 215 ± 34 mm^3, and the mean response amplitude over these voxels in each LGN was 0.72 ± 0.03% for the motion stimulus and 1.50 ± 0.06% for the checkerboard stimulus, a significant difference ($t_7 = 10.3$, $P = 0.000018$). The amplitudes evoked by the motion and flickering checkerboard stimuli have been plotted against each other for each individual voxel in the LGN in Fig. 6*C*. The slope of the linear regression line was 0.49. Although the flickering checkerboard evoked stronger responses than the motion stimulus in both the SC and LGN, the motion stimulus evoked a relatively stronger response in the SC than in the LGN.

To study whether differences in eye movement patterns during the viewing of the stimuli could have caused the greater SC response to motion, we monitored the gaze position for three subjects while they fixated and passively viewed the moving and static dots stimulus during six scanning runs each. The contrast between the moving and static dot stimuli activated a mean SC volume of 189 ± 16 mm^3 and evoked a mean response amplitude of 0.77 ± 0.06%. These values were not significantly different ($t_5 = 1.08$, $P = 0.32$ and $t_5 = 0.08$, $P = 0.94$, respectively) than the mean volume of 263 ± 57 mm^3

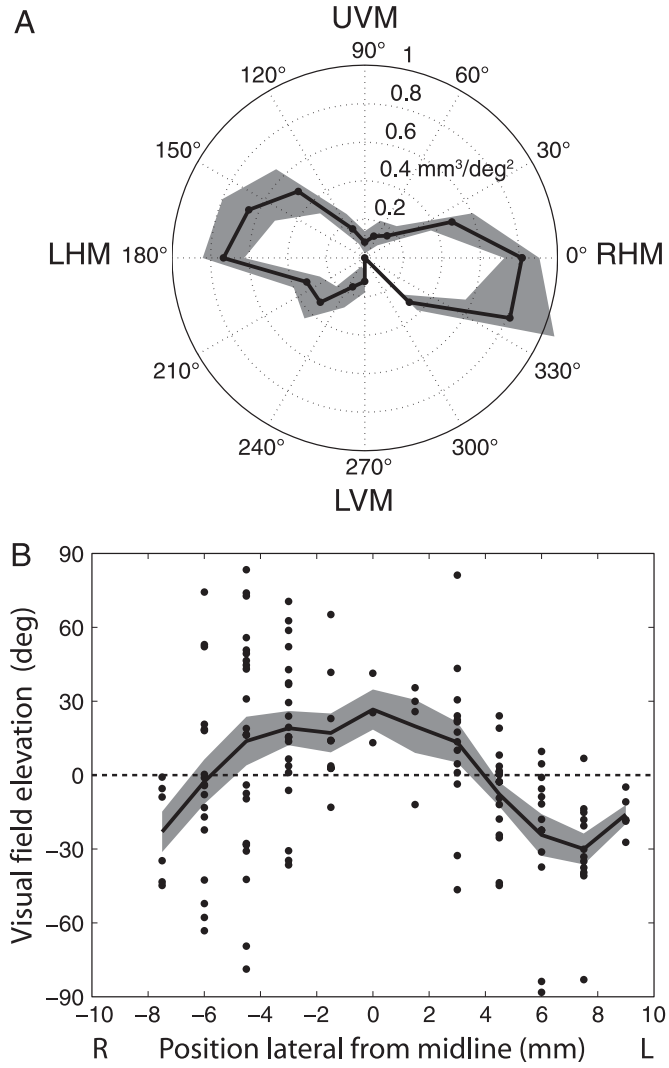

FIG. 5. Polar angle representation in the SC. *A*: representations in the SC of the visual field at different polar angles were measured for the central 15° of eccentricity by dividing the visual field into 16 sectors and sorting voxels activated by the rotating hemifield stimulus according to phase responses into each sector. Results for the left and right SC are shown combined. No ipsilateral activity was observed—points in the right (left) visual field correspond to the representation in the left (right) SC. Points and lines trace mean volume per unit area of the visual field for each of the sectors, averaged over subjects ($n = 5$). Gray regions indicate range of SE. Upper (UVM) and lower (LVM) vertical meridians are significantly underrepresented relative to the left (LHM) and right (RHM) horizontal meridians. *B*: distance of each voxel from the midline of the midbrain is plotted against the elevation in the visual field represented by the voxel. Positive distances are in the left (L) hemisphere and negative distances are in the right (R) hemisphere. Each point represents 1 SC voxel. Solid black line indicates mean across all voxels at each position for all subjects, and the extent of the surrounding gray field indicates SE. Dotted line indicates 0° of elevation, the horizontal meridian. Medial to lateral positions within the SC systematically tend to represent upper to lower elevations in the visual field.

and mean amplitude of 0.76 ± 0.08% observed during the four sessions during which eye movements were not monitored. Across all scanning runs, the mean gaze distance from the center of fixation was 1.52 ± 0.13° during the static blocks and 1.44 ± 0.11° during the motion blocks. These values did not differ significantly (paired 2-tailed *t*-test, $t_{17} = 1.37$, $P = 0.19$). Similarly, the dispersion of the gaze position was not significantly different between the moving and static blocks ($t_{17} = 0.94$, $P = 0.36$); the mean of the SD of the horizontal and vertical gaze positions was 1.36 ± 0.09° during the static blocks and 1.29 ± 0.09° during the motion blocks. The mean gaze speed, consisting mainly of small amplitude jitter, was significantly larger during the static blocks, 7.82 ± 0.22°/s, than during the motion blocks, 6.59 ± 0.26°/s ($t_{17} = 5.07$, $P = 0.000094$). The mean pupil diameter was significantly smaller during the static blocks, 5.28 ± 0.19 mm, than during the motion blocks, 5.85 ± 0.18 mm ($t_{17} = -17.5$, $P = 2.5 \times 10^{-12}$). There were significantly more eye blinks during the static blocks than during the motion blocks, 19.3 ± 1.6 (1 blink per 6.6 s) versus 8.6 ± 1.4 (1 blink per 14.7 s), respectively ($t_{17} = 5.52$, $P = 0.000037$). Although the pattern of small eye

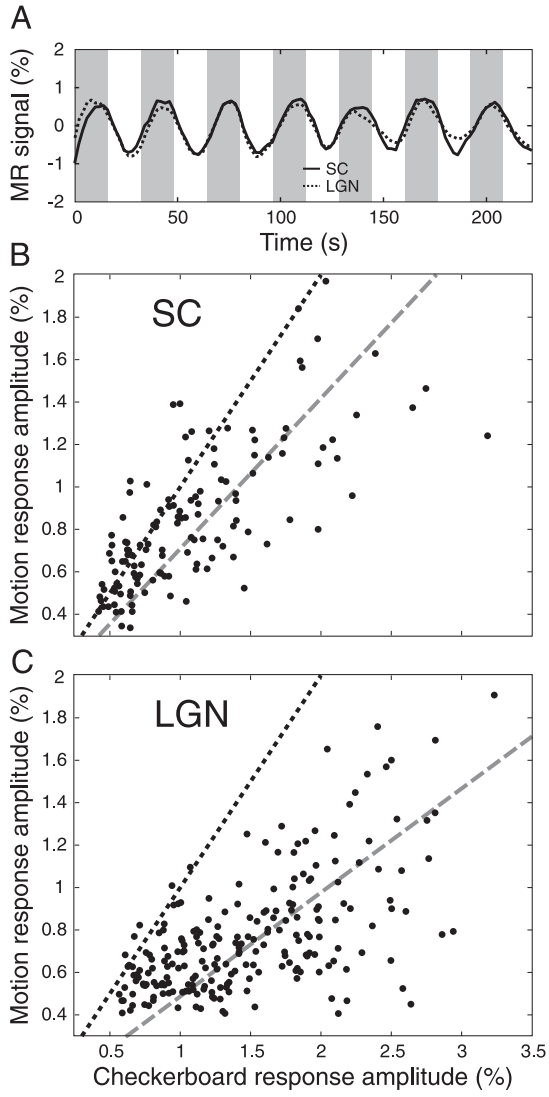

FIG. 6. Motion responses. *A*: mean fMRI time series of voxels activated by the motion stimulus are shown averaged over both SC (solid line) or LGN (dotted line) in 4 subjects. Gray fields indicate periods during which dots in the stimulus were moving. Stationary dots were presented interleaved. *B* and *C*: for each voxel in the SC (*B*) and LGN (*C*) activated by both the flickering checkerboard and moving vs. static dots stimuli, response amplitudes for the two stimuli are plotted against each other. Dotted black line indicates equal response amplitudes for the two stimuli. Dashed gray line indicates regression line. Slope for the SC line was 0.71, and slope for the LGN line was 0.49. Relative to the checkerboard stimulus, motion stimulus activated the SC more optimally than the LGN.

movements differed between the motion and static blocks, the movements occurred more frequently during the static blocks and therefore cannot account for our finding of a stronger response in the SC during the motion blocks.

DISCUSSION

Using high-resolution fMRI at 3 T, we identified regions in the roof of the midbrain that were activated by flickering checkerboard and moving dot stimuli. These activations likely originated from the superficial layers of the SC. The SC regions represented the contralateral visual hemifield, with the upper to lower regions of the visual field represented along the medial to lateral direction. No reliable map of eccentricity could be systematically observed. The human SC exhibited high sensitivity to low stimulus contrast and also responded well to stimulus motion.

Contrast response

The SC responded to luminance contrast as low as 5% and exhibited a shallow contrast response function. The magnitude of the contrast modulation was similar throughout the extent of the SC. Thus the SC was well activated by low stimulus contrast and only weakly modulated by changes in stimulus contrast.

Unlike many other response properties of the SC, its contrast response function has not been thoroughly studied in primates. Neurons in the superficial layers of the SC respond well to transient luminance-defined stimuli and have been generally thought to be insensitive to stimulus luminance contrast (see Bisti and Sireteanu 1976; Marrocco and Li 1977), but contrast response functions have not been reported in primates. Single-cell physiology studies performed in the cat have reported that the responses of the vast majority of SC neurons increase with contrast (Bisti and Sireteanu 1976; Pinter and Harris 1981). It is difficult, however, to estimate the population response to stimulus contrast from these studies. Contrast response functions were reported only for individual neurons and showed considerable variability, with some neurons responding to contrast as low as 5% and others only to contrast >30%. Saturated responses were typically found at contrast of 15–30%. Our results suggest that the population response of neurons in the superficial layers is nearly saturated in response to stimuli with contrast of 10%. Our finding that a large change in contrast evokes only a small change in the population response is consistent with the view that the SC response is largely invariant to stimulus contrast (Bisti and Sireteanu 1976; Marrocco and Li 1977).

In comparison with the SC, the LGN response was found to be more strongly modulated by stimulus contrast (see also Kastner et al. 2004) and more heterogeneous in the range of contrast responses present throughout its structure (Schneider et al. 2004). In addition to voxels that responded to low stimulus contrast and were only weakly modulated by increases in stimulus contrast similar to those found in the SC, other voxels were found in the LGN that were strongly modulated by stimulus contrast. We have suggested that the weakly and strongly contrast-modulated parts of the LGN correspond to the two populations of magnocellular (M) and parvocellular (P) neurons in the LGN (Schneider et al. 2004). In contrast, the SC appears to contain a more homogenous population with responses similar to the M-LGN.

The similarity between the contrast responses of the presumed M portions of the human LGN and the human SC warrants a discussion of their retinal afferents and interconnectivity. Retinal ganglion cells with large cell bodies, medium-sized dendritic fields and Y-like response properties, known as parasol, B, or Pβ, project to the M layers of the LGN (de Monasterio 1978a; Leventhal et al. 1981; Perry and Cowey 1981; Perry et al. 1984; Schiller and Malpeli 1977). However, in the macaque, parasol cells project to the SC only extremely rarely (Perry and Cowey 1984; Rodieck and Watanabe 1993). The majority of the retinotectal projections arise from a number of distinct cell types—some have been labeled Pγ, Pϵ, and C—with heterogeneous morphology and response properties (de Monasterio 1978b; Leventhal et al. 1981; Marrocco and Li 1977; Perry and Cowey 1984; Rodieck and Watanabe 1993; Schiller and Malpeli 1977). These afferents include W-like cells that have relatively poor contrast sensitivity, as shown in the cat LGN (Sur and Sherman 1982), and therefore are unlikely to drive the high contrast sensitivity that we observed. The contrast sensitivity of the other retinal projections to the SC has not been well studied.

Despite the apparent lack of shared retinal afferents, the SC and M-LGN are functionally connected. The M but not P layers of the LGN project to the SC indirectly through a corticotectal pathway (Hoffmann 1973). Inactivation of the visual cortex or M layers of the LGN disrupts the visually driven activity in the deep but not in the superficial layers of the SC, whereas inactivation of the P layers of the LGN has no effect on either part of the SC (Schiller et al. 1974, 1979). These corticotectal neurons likely play only a modulatory role in gating the transmission of information from the superior to deep layers of the SC, because they lack the responses related to eye movements and novel stimuli that are found in deep layers of the SC and are therefore unlikely to impart these properties (Finlay et al. 1976). The SC does send efferents to the LGN, but not directly to the M layers. In the squirrel monkey, the superficial layers of the SC have been reported to project to both the koniocellular (K) layers, also known as the interlaminar zones, and M layers of the LGN (Harting et al. 1978), but subsequent observations in the macaque and other species indicated that the SC projections were confined to the K layers, primarily the ventral ones near the M layers (Harting et al. 1991). In summary, although the M-LGN and SC are functionally connected, it is not clear that this interconnectivity could explain their similar contrast response properties.

Retinotopy

In the macaque, the visual field is represented orderly in the superficial layers of the SC. In each SC, neurons respond exclusively to visual stimuli presented in the contralateral hemifield. The upper and lower visual field are represented medially and laterally, respectively, and the fovea and periphery are represented anteriorly and posteriorly (Cynader and Berman 1972; Goldberg and Wurtz 1972a). The central 10° are relatively overrepresented, as in other areas of the visual system, and occupy over one-third of the SC surface area (Cynader and Berman 1972). Confirming the overall topographic organization in the human, we found that responses of

each SC were restricted to stimulation of the contralateral hemifield. We also observed a lateral to medial representation of the lower to upper visual field. The horizontal meridian was overrepresented relative to the vertical meridian, qualitatively similar to findings in the human LGN (Schneider et al. 2004) and area V1 of the visual cortex (Janik et al. 2003). Partial volume effects (Haacke et al. 1994; Logothetis et al. 2002) may at least partially account for the underrepresentation of the vertical meridian, because the upper and lower vertical meridians are represented along the medial and lateral edges of the SC. However, given the magnitude of the underrepresentation and the finding that SC activity typically extended to the anatomical borders of the midbrain, partial volume effects are unlikely to explain the distortion entirely. The potentially large sizes of receptive fields in SC neurons may provide a better explanation. Given the spatial resolution used in this study, the signals observed in each SC voxel likely originated from multiple layers of the SC. In the macaque SC, receptive field sizes increase with eccentricity, ranging from $<1°$ in the fovea to as large as a quadrant in the periphery, and also with depth from the surface of the SC (Cynader and Berman 1972; Goldberg and Wurtz 1972a; Humphrey 1968; Marrocco and Li 1977; Schiller and Koerner 1971). Because SC neurons respond strictly to stimulation of the contralateral visual field, the larger their receptive fields, the further their centers must be located from the vertical meridian. Otherwise, large receptive fields with centers near the vertical meridian would overlap into the ipsilateral visual field. The retinotopic mapping procedure used in this study locates the visual field representation of a voxel depending on the center of its response. For example, a voxel that was responsive to stimuli within an entire hemifield would be mapped onto the horizontal meridian. Large receptive fields may also explain the poor responses to the expanding ring stimulus, for which the active portions of the stimulus were continuously present in each visual field, separated by a 7.5° gap. The stimulus would not have modulated the activity of neurons with receptive fields larger than this gap. Most of the activity evoked by the expanding ring stimulus was found foveally, where receptive fields would be smaller, and an anterior to posterior map of increasing eccentricity was found in only 2 of 14 SC.

The retinotopic organization found in the SC was not as detailed as that recently shown in the human LGN. Using the same high-resolution technique and traveling wave stimuli as in this study, we were able to map the central 15° of the visual field in the LGN (Schneider et al. 2004). It was found that the contralateral field was represented with the lower field in the medial-superior portion and the upper field in the lateral-inferior portion of each LGN. The fovea was represented in posterior and superior portions, with increasing eccentricities represented more anteriorly. Importantly, the magnocellular parts of the LGN were identified in its inferior and medial portions based on their sensitivity to low stimulus contrast.

Two primary factors may account for the difficulty in observing more detailed retinotopic maps in the SC in some subjects. First, the activated SC volume was approximately one-fifth of the activated LGN volume. In this study, a rotating hemifield stimulus activated a mean individual SC volume of 86 ± 14 mm^3, whereas in the same five subjects, the mean individual LGN volume activated by the identical stimulus was 437 ± 36 mm^3. Displaying stimuli in a larger fraction of the visual field may increase the activated volume significantly in the SC, because the activated portion of the SC likely occupied a smaller fraction of the overall SC volume than did the activated portion of the LGN. Although the central 10° are relatively overrepresented in the SC, as in other visual structures and areas, occupying over one-third of the SC surface area in macaques (Cynader and Berman 1972), the representation of the central 10° in the human LGN is greatly expanded and estimated to occupy 73% of the total LGN volume (Schneider et al. 2004). Second, signal degrading imaging artifacts caused by cardiovascular pulsations and tissue boundaries may be more prominent near the SC than near the LGN. These factors may contribute to the lack of detail in the polar angle component of the retinotopic map in the SC and, in addition to the discussion of receptive field sizes above, may explain the lack of activation by the eccentricity stimulus.

Response to motion

The human SC was well activated by both a high contrast flickering checkerboard and a field of radially moving dots of slow velocity, with slightly stronger responses evoked by the checkerboard stimulus. The SC in other species has also been found to be particularly responsive to moving stimuli. Neurons in the superficial layers are broadly tuned to velocity. Many cells, especially those with large receptive fields, were found to respond to high stimulus velocities of 800–900°/s, similar to saccade peak velocities (Cynader and Berman 1972; Goldberg and Wurtz 1972a; Marrocco and Li 1977; Robinson and Wurtz 1976). Almost all cells were well activated by stimulus velocities of 5°/s (Marrocco and Li 1977), consistent with these findings of SC activation with a dot field moving at 7°/s. Only a small fraction of neurons that responded to stimulus motion in the superficial layers were found to be selective for direction (Cynader and Berman 1972; Goldberg and Wurtz 1972a; Marrocco and Li 1977; Schiller and Koerner 1971), although most were selective for velocity relative to a moving background (Davidson and Bender 1991). Similar to those in the superficial layers, SC neurons in the deeper layers responded well to both moving and flickering stationary stimuli and were not particularly sensitive to direction or speed of motion (Krauzlis 2004a; Marrocco and Li 1977). Only about 14% of these cells may be considered motion sensitive, that is, responding better to moving dots than to stationary flickering dots and exhibiting velocity tuning. Consistent with the findings in macaques, we observed a preference of the human SC population for the flickering checkerboard versus the moving dots stimulus, and it is likely that the general transient nature of the motion stimulus rather than its specific motion coherence was the primary driver of this population response. It is also possible that neurons responsive to transients quickly adapt to sustained stimuli such as the static dot field we used as a contrast to the motion stimulus, which may exaggerate response differences between the two stimuli. Transient and moving stimuli are both important targets for eye movements, and the SC population responds well to both. In addition, the SC has also been implicated in the initiation of smooth-pursuit eye movements (Basso et al. 2000; Krauzlis 2003; Krauzlis et al. 2000; Munoz and Wurtz 1993, 1995), for which the motion sensitive neurons would be instrumental.

Several potential confounds need to be considered in a discussion of the motion sensitivity of the SC. One concern might be that the stability of the subjects' fixation varied between motion and static presentation blocks. Given the prominent involvement of the SC in eye movements and fixation, more frequent eye movements could produce greater fMRI activation. However, we observed the opposite, that in fact the gaze position was more stable during the motion than the static blocks. This finding may indicate that the subjects' arousal or attentional state differed between presentations of moving and static stimuli. The subjects may have been trying harder to maintain fixation or pay attention during the motion presentations or the motion stimulus may have automatically captured attention. Several behavioral measures tend to support this interpretation, including the differences in fixational stability. Subjects' pupil size was larger during the motion blocks than during the static presentations. The change in pupil size may simply reflect the greater luminance of the static dots because of the temporal characteristics of the LCD video projector used to display the stimuli. However, it is possible that the pupils dilated during the motion blocks because of an increased state of vigilance in the subjects (Hakerem and Sutton 1966; Hess and Polt 1960). In addition, the smaller number of blinks during the motion blocks may be indicative of subjects' increased effort or concentration. Given our measurements, we cannot rule out that attention could be in part responsible for the different responses evoked by moving and static stimuli. This potential confound is common to many reports of motion related fMRI activity (e.g., Huk et al. 2001). Eye blinks have been reported to suppress the activity of saccade-related burst neurons in the intermediate and deep layers of the SC (Goossens and Van Opstal 2000) as well as sustained and, most prominently, transient activity in V1 (Gawne and Martin 2000). Although there was likely little saccade-related or transient stimulus-related activity during the static blocks, we cannot rule out the possibility that the increased blink frequency during the static block may have affected the hemodynamic response.

A number of studies have examined motion responsive regions in the human brain using moving versus static dot fields and other motion stimuli. Some of these studies investigated specific cortical areas and used scanning volumes that excluded the SC and LGN. However, a number of studies did acquire volumes that included the SC and LGN, but none have reported SC or LGN activity (Cheng et al. 1995; Claeys et al. 2003; Cornette et al. 1998; Dukelow et al. 2001; Dupont et al. 1994, 1997; Hampson et al. 2004; O'Craven et al. 1997; Shulman et al. 1998, 1999; Sunaert et al. 1999; Van Oostende et al. 1997; Zeki et al. 1991). The lower spatial resolution used in many of these studies, typically $>3 \times 3 \times 3$ mm^3, may account for these negative findings (Hyde et al. 2001). Other factors that may also have contributed to a weaker signal from the small, deep, subcortical SC and LGN, include the use of PET scanners or lower field strength (1.5 T) MRI scanners, spatial smoothing of the MRI data, and/or the use of an MR surface coil.

ACKNOWLEDGMENTS

We thank H. M. Fehd for assistance.

GRANTS

This study was supported by National Institute of Mental Health Grants R01MH-64043, P50MH-62196, and T32 MH-065214 and by a grant from the Whitehall Foundation.

REFERENCES

Astruc J. Corticofugal connections of area 8 (frontal eye field) in Macaca mulatta. *Brain Res* 33: 241–256, 1971.

Bandettini PA, Jesmanowicz A, Wong EC, and Hyde JS. Processing strategies for time-course data sets in functional MRI of the human brain. *Magn Reson Med* 30: 161–173, 1993.

Basso MA, Krauzlis RJ, and Wurtz RH. Activation and inactivation of rostral superior colliculus neurons during smooth-pursuit eye movements in monkeys. *J Neurophysiol* 84: 892–908, 2000.

Bisti S and Sireteanu RC. Sensitivity to spatial frequency and contrast of visual cells in the cat superior colliculus. *Vision Res* 16: 247–251, 1976.

Brainard DH. The psychophysics toolbox. *Spat Vis* 10: 433–436, 1997.

Büchel C, Josephs O, Rees G, Turner R, Frith CD, and Friston KJ. The functional anatomy of attention to visual motion. A functional MRI study. *Brain* 121: 1281–1294, 1998.

Cheng K, Fujita H, Kanno I, Miura S, and Tanaka K. Human cortical regions activated by wide-field visual motion: an H2(15)O PET study. *J Neurophysiol* 74: 413–427, 1995.

Claeys KG, Lindsey DT, De Schutter E, and Orban GA. A higher order motion region in human inferior parietal lobule: evidence from fMRI. *Neuron* 40: 631–642, 2003.

Corbetta M, Miezin FM, Dobmeyer S, Shulman GL, and Petersen SE. Selective and divided attention during visual discriminations of shape, color, and speed: functional anatomy by positron emission tomography. *J Neurosci* 11: 2383–2402, 1991.

Cornette L, Dupont P, Rosier A, Sunaert S, Van Hecke P, Michiels J, Mortelmans L, and Orban GA. Human brain regions involved in direction discrimination. *J Neurophysiol* 79: 2749–2765, 1998.

Cynader M and Berman N. Receptive-field organization of monkey superior colliculus. *J Neurophysiol* 35: 187–201, 1972.

Davidson RM and Bender DB. Selectivity for relative motion in the monkey superior colliculus. *J Neurophysiol* 65: 1115–1133, 1991.

de Monasterio FM. Properties of concentrically organized X and Y ganglion cells of macaque retina. *J Neurophysiol* 41: 1394–1417, 1978a.

de Monasterio FM. Properties of ganglion cells with atypical receptive-field organization in retina of macaques. *J Neurophysiol* 41: 1435–1449, 1978b.

DeYoe EA, Bandettini P, Neitz J, Miller D, and Winans P. Functional magnetic resonance imaging (FMRI) of the human brain. *J Neurosci Methods* 54: 171–187, 1994.

DeYoe EA, Carman GJ, Bandettini P, Glickman S, Wieser J, Cox R, Miller D, and Neitz J. Mapping striate and extrastriate visual areas in human cerebral cortex. *Proc Natl Acad Sci USA* 93: 2382–2386, 1996.

DuBois RM and Cohen MS. Spatiotopic organization in human superior colliculus observed with fMRI. *Neuroimage* 12: 63–70, 2000.

Dukelow SP, DeSouza JF, Culham JC, van den Berg AV, Menon RS, and Vilis T. Distinguishing subregions of the human MT+ complex using visual fields and pursuit eye movements. *J Neurophysiol* 86: 1991–2000, 2001.

Dupont P, De Bruyn B, Vandenberghe R, Rosier AM, Michiels J, Marchal G, Mortelmans L, and Orban GA. The kinetic occipital region in human visual cortex. *Cereb Cortex* 7: 283–292, 1997.

Dupont P, Orban GA, De Bruyn B, Verbruggen A, and Mortelmans L. Many areas in the human brain respond to visual motion. *J Neurophysiol* 72: 1420–1424, 1994.

Engel SA, Glover GH, and Wandell BA. Retinotopic organization in human visual cortex and the spatial precision of functional MRI. *Cereb Cortex* 7: 181–192, 1997.

Engel SA, Rumelhart DE, Wandell BA, Lee AT, Glover GH, Chichilnisky EJ, and Shadlen MN. fMRI of human visual cortex. *Nature* 369: 525, 1994.

Finlay BL, Schiller PH, and Volman SF. Quantitative studies of single-cell properties in monkey striate cortex. IV. Corticotectal cells. *J Neurophysiol* 39: 1352–1361, 1976.

Fries W. Cortical projections to the superior colliculus in the macaque monkey: a retrograde study using horseradish peroxidase. *J Comp Neurol* 230: 55–76, 1984.

Fries W and Distel H. Large layer VI neurons of monkey striate cortex (Meynert cells) project to the superior colliculus. *Proc R Soc Lond B Biol Sci* 219: 53–59, 1983.

Gawne TJ and Martin JM. Activity of primate V1 cortical neurons during blinks. *J Neurophysiol* 84: 2691–2694, 2000.

Gitelman DR, Parrish TB, Friston KJ, and Mesulam MM. Functional anatomy of visual search: regional segregations within the frontal eye fields and effective connectivity of the superior colliculus. *Neuroimage* 15: 970–982, 2002.

Goldberg ME and Wurtz RH. Activity of superior colliculus in behaving monkey. I. Visual receptive fields of single neurons. *J Neurophysiol* 35: 542–559, 1972a.

Goldberg ME and Wurtz RH. Activity of superior colliculus in behaving monkey. II. Effect of attention on neuronal responses. *J Neurophysiol* 35: 560–574, 1972b.

Goldman PS and Nauta WJ. Autoradiographic demonstration of a projection from prefrontal association cortex to the superior colliculus in the rhesus monkey. *Brain Res* 116: 145–149, 1976.

Goossens HH and Van Opstal AJ. Blink-perturbed saccades in monkey. II. Superior colliculus activity. *J Neurophysiol* 83: 3430–3452, 2000.

Graham J. Some topographical connections of the striate cortex with subcortical structures in Macaca fascicularis. *Exp Brain Res* 47: 1–14, 1982.

Graybiel AM. Periodic-compartmental distribution of acetylcholinesterase in the superior colliculus of the human brain. *Neuroscience* 4: 643–650, 1979.

Grön G, Wunderlich AP, Spitzer M, Tomczak R, and Riepe MW. Brain activation during human navigation: gender-different neural networks as substrate of performance. *Nat Neurosci* 3: 404–408, 2000.

Guimaraes AR, Melcher JR, Talavage TM, Baker JR, Ledden P, Rosen BR, Kiang NY, Fullerton BC, and Weisskoff RM. Imaging subcortical auditory activity in humans. *Hum Brain Mapp* 6: 33–41, 1998.

Haacke EM, Hopkins A, Lai S, Buckley P, Friedman L, Meltzer H, Hedera P, Friedland R, Klein S, Thompson L, Detterman D, Tkach J, and Lewin JS. 2D and 3D high resolution gradient echo functional imaging of the brain: venous contributions to signal in motor cortex studies. *NMR Biomed* 7: 54–62, 1994.

Hakerem G and Sutton S. Pupillary response at visual threshold. *Nature* 212: 485–486, 1966.

Hampson M, Olson IR, Leung HC, Skudlarski P, and Gore JC. Changes in functional connectivity of human MT/V5 with visual motion input. *Neuroreport* 15: 1315–1319, 2004.

Harting JK, Casagrande VA, and Weber JT. The projection of the primate superior colliculus upon the dorsal lateral geniculate nucleus: autoradiographic demonstration of interlaminar distribution of tectogeniculate axons. *Brain Res* 150: 593–599, 1978.

Harting JK, Huerta MF, Hashikawa T, and van Lieshout DP. Projection of the mammalian superior colliculus upon the dorsal lateral geniculate nucleus: organization of tectogeniculate pathways in nineteen species. *J Comp Neurol* 304: 275–306, 1991.

Hess EH and Polt JM. Pupil size as related to interest value of visual stimuli. *Science* 132: 349–350, 1960.

Hilbig H, Bidmon HJ, Zilles K, and Busecke K. Neuronal and glial structures of the superficial layers of the human superior colliculus. *Anat Embryol (Berl)* 200: 103–115, 1999.

Hoffmann KP. Conduction velocity in pathways from retina to superior colliculus in the cat: a correlation with receptive-field properties. *J Neurophysiol* 36: 409–424, 1973.

Huk AC, Ress D, and Heeger DJ. Neuronal basis of the motion aftereffect reconsidered. *Neuron* 32: 161–172, 2001.

Humphrey NK. Responses to visual stimuli of units in the superior colliculus of rats and monkeys. *Exp Neurol* 20: 312–340, 1968.

Hyde JS, Biswal BB, and Jesmanowicz A. High-resolution fMRI using multislice partial k-space GR-EPI with cubic voxels. *Magn Reson Med* 46: 114–125, 2001.

Ignashchenkova A, Dicke PW, Haarmeier T, and Thier P. Neuron-specific contribution of the superior colliculus to overt and covert shifts of attention. *Nat Neurosci* 7: 56–64, 2004.

Janik JJ, Ropella KM, and DeYoe EA. Distortions of human retinotopy obtained with temporal phase mapped fMRI. *Soc Neurosci Abstr* 29: 658, 2003.

Jenkinson M, Bannister P, Brady M, and Smith S. Improved optimisation for the robust and accurate linear registration and motion correction of brain images. *Neuroimage* 17: 825–841, 2002.

Kastner S, O'Connor DH, Fukui MM, Fehd HM, Herwig U, and Pinsk MA. Functional imaging of the human lateral geniculate nucleus and pulvinar. *J Neurophysiol* 91: 438–448, 2004.

Komatsu H and Suzuki H. Projections from the functional subdivisions of the frontal eye field to the superior colliculus in the monkey. *Brain Res* 327: 324–327, 1985.

Krauzlis RJ. Neuronal activity in the rostral superior colliculus related to the initiation of pursuit and saccadic eye movements. *J Neurosci* 23: 4333–4344, 2003.

Krauzlis RJ. Activity of rostral superior colliculus neurons during passive and active viewing of motion. *J Neurophysiol* 92: 949–958, 2004a.

Krauzlis RJ. Recasting the smooth pursuit eye movement system. *J Neurophysiol* 91: 591–603, 2004b.

Krauzlis RJ, Basso MA, and Wurtz RH. Discharge properties of neurons in the rostral superior colliculus of the monkey during smooth-pursuit eye movements. *J Neurophysiol* 84: 876–891, 2000.

Kunzle H and Akert K. Efferent connections of cortical, area 8 (frontal eye field) in Macaca fascicularis. A reinvestigation using the autoradiographic technique. *J Comp Neurol* 173: 147–164, 1977.

Kunzle H, Akert K, and Wurtz RH. Projection of area 8 (frontal eye field) to superior colliculus in the monkey. An autoradiographic study. *Brain Res* 117: 487–492, 1976.

Kustov AA and Robinson DL. Shared neural control of attentional shifts and eye movements. *Nature* 384: 74–77, 1996.

Kuypers HG and Lawrence DG. Cortical projections to the red nucleus and the brain stem in the Rhesus monkey. *Brain Res* 4: 151–188, 1967.

Laemle LKA. Golgi study of cellular morphology in the superficial layers of superior colliculus of man, *Saimiri*, and *Macaca. J Hirnforsch* 22: 253–263, 1981.

Laemle LKA. Golgi study of cell morphology in the deep layers of the human superior colliculus. *J Hirnforsch* 24: 297–306, 1983.

Leichnetz GR, Spencer RF, Hardy SG, and Astruc J. The prefrontal corticotectal projection in the monkey; an anterograde and retrograde horseradish peroxidase study. *Neuroscience* 6: 1023–1041, 1981.

Leuba G and Saini K. Calcium-binding proteins immunoreactivity in the human subcortical and cortical visual structures. *Vis Neurosci* 13: 997–1009, 1996.

Leventhal AG, Rodieck RW, and Dreher B. Retinal ganglion cell classes in the Old World monkey: morphology and central projections. *Science* 213: 1139–1142, 1981.

Logothetis N, Merkle H, Augath M, Trinath T, and Ugurbil K. Ultra high-resolution fMRI in monkeys with implanted RF coils. *Neuron* 35: 227–242, 2002.

Lynch JC, Graybiel AM, and Lobeck LJ. The differential projection of two cytoarchitectonic subregions of the inferior parietal lobule of macaque upon the deep layers of the superior colliculus. *J Comp Neurol* 235: 241–254, 1985.

Marrocco RT and Li RH. Monkey superior colliculus: properties of single cells and their afferent inputs. *J Neurophysiol* 40: 844–860, 1977.

Moschovakis AK, Scudder CA, and Highstein SM. The microscopic anatomy and physiology of the mammalian saccadic system. *Prog Neurobiol* 50: 133–254, 1996.

Munoz DP and Wurtz RH. Fixation cells in monkey superior colliculus. I. Characteristics of cell discharge. *J Neurophysiol* 70: 559–575, 1993.

Munoz DP and Wurtz RH. Saccade-related activity in monkey superior colliculus. I. Characteristics of burst and buildup cells. *J Neurophysiol* 73: 2313–2333, 1995.

O'Craven KM, Rosen BR, Kwong KK, Treisman A, and Savoy RL. Voluntary attention modulates fMRI activity in human MT-MST. *Neuron* 18: 591–598, 1997.

Pelli DG. The VideoToolbox software for visual psychophysics: transforming numbers into movies. *Spat Vis* 10: 437–442, 1997.

Perry VH and Cowey A. The morphological correlates of X- and Y-like retinal ganglion cells in the retina of monkeys. *Exp Brain Res* 43: 226–228, 1981.

Perry VH and Cowey A. Retinal ganglion cells that project to the superior colliculus and pretectum in the macaque monkey. *Neuroscience* 12: 1125–1137, 1984.

Perry VH, Oehler R, and Cowey A. Retinal ganglion cells that project to the dorsal lateral geniculate nucleus in the macaque monkey. *Neuroscience* 12: 1101–1123, 1984.

Petit L and Beauchamp MS. Neural basis of visually guided head movements studied with fMRI. *J Neurophysiol* 89: 2516–2527, 2003.

Pinter RB and Harris LR. Temporal and spatial response characteristics of the cat superior colliculus. *Brain Res* 207: 73–94, 1981.

Poncelet BP, Wedeen VJ, Weisskoff RM, and Cohen MS. Brain parenchyma motion: measurement with cine echo-planar MR imaging. *Radiology* 185: 645–651, 1992.

Robinson DL and Jarvis CD. Superior colliculus neurons studied during head and eye movements of the behaving monkey. *J Neurophysiol* 37: 533–540, 1974.

Robinson DL and Kertzman C. Covert orienting of attention in macaques. III. Contributions of the superior colliculus. *J Neurophysiol* 74: 713–721, 1995.

Robinson DL and Wurtz RH. Use of an extraretinal signal by monkey superior colliculus neurons to distinguish real from self-induced stimulus movement. *J Neurophysiol* 39: 852–870, 1976.

Rodieck RW and Watanabe M. Survey of the morphology of macaque retinal ganglion cells that project to the pretectum, superior colliculus, and parvicellular laminae of the lateral geniculate nucleus. *J Comp Neurol* 338: 289–303, 1993.

Schiller PH and Koerner F. Discharge characteristics of single units in superior colliculus of the alert rhesus monkey. *J Neurophysiol* 34: 920–936, 1971.

Schiller PH and Malpeli JG. Properties and tectal projections of monkey retinal ganglion cells. *J Neurophysiol* 40: 428–445, 1977.

Schiller PH, Malpeli JG, and Schein SJ. Composition of geniculostriate input to superior colliculus of the rhesus monkey. *J Neurophysiol* 42: 1124–1133, 1979.

Schiller PH and Stryker M. Single-unit recording and stimulation in superior colliculus of the alert rhesus monkey. *J Neurophysiol* 35: 915–924, 1972.

Schiller PH, Stryker M, Cynader M, and Berman N. Response characteristics of single cells in the monkey superior colliculus following ablation or cooling of visual cortex. *J Neurophysiol* 37: 181–194, 1974.

Schmitz B, Kasmann-Kellner B, Schafer T, Krick CM, Gron G, Backens M, and Reith W. Monocular visual activation patterns in albinism as revealed by functional magnetic resonance imaging. *Hum Brain Mapp* 23: 40–52, 2004.

Schneider KA, Richter MC, and Kastner S. Retinotopic organization and functional subdivisions of the human lateral geniculate nucleus: a high-resolution functional magnetic resonance imaging study. *J Neurosci* 24: 8975–8985, 2004.

Segraves MA and Goldberg ME. Functional properties of corticotectal neurons in the monkey's frontal eye field. *J Neurophysiol* 58: 1387–1419, 1987.

Sereno MI, Dale AM, Reppas JB, Kwong KK, Belliveau JW, Brady TJ, Rosen BR, and Tootell RB. Borders of multiple visual areas in humans revealed by functional magnetic resonance imaging. *Science* 268: 889–893, 1995.

Shulman GL, Ollinger JM, Akbudak E, Conturo TE, Snyder AZ, Petersen SE, and Corbetta M. Areas involved in encoding and applying directional expectations to moving objects. *J Neurosci* 19: 9480–9496, 1999.

Shulman GL, Schwarz J, Miezin FM, and Petersen SE. Effect of motion contrast on human cortical responses to moving stimuli. *J Neurophysiol* 79: 2794–2803, 1998.

Sommer MA and Wurtz RH. Composition and topographic organization of signals sent from the frontal eye field to the superior colliculus. *J Neurophysiol* 83: 1979–2001, 2000.

Sparks DL. Response properties of eye movement-related neurons in the monkey superior colliculus. *Brain Res* 90: 147–152, 1975.

Sparks DL. Translation of sensory signals into commands for control of saccadic eye movements: role of primate superior colliculus. *Physiol Rev* 66: 118–171, 1986.

Sparks DL. The brainstem control of saccadic eye movements. *Nat Rev Neurosci* 3: 952–964, 2002.

Sunaert S, Van Hecke P, Marchal G, and Orban GA. Motion-responsive regions of the human brain. *Exp Brain Res* 127: 355–370, 1999.

Sur M and Sherman SM. Linear and nonlinear W-cells in C-laminae of the cat's lateral geniculate nucleus. *J Neurophysiol* 47: 869–884, 1982.

Talairach J and Tournoux P. *Stereotactic Coplanar Atlas of the Human Brain.* New York: Thieme Medical, 1988.

Tardif E and Clarke S. Commissural connections of human superior colliculus. *Neuroscience* 111: 363–372, 2002.

Van Oostende S, Sunaert S, Van Hecke P, Marchal G, and Orban GA. The kinetic occipital (KO) region in man: an fMRI study. *Cereb Cortex* 7: 690–701, 1997.

Wallace MN. Lattices of high histochemical activity occur in the human, monkey, and cat superior colliculus. *Neuroscience* 25: 569–583, 1988.

Wilson ME and Toyne MJ. Retino-tectal and cortico-tectal projections in Macaca mulatta. *Brain Res* 24: 395–406, 1970.

Woods RP, Grafton ST, Holmes CJ, Cherry SR, and Mazziotta JC. Automated image registration. I. General methods and intrasubject, intramodality validation. *J Comput Assist Tomogr* 22: 139–152, 1998.

Wurtz RH and Albano JE. Visual-motor function of the primate superior colliculus. *Annu Rev Neurosci* 3: 189–226, 1980.

Wurtz RH and Goldberg ME. Superior colliculus cell responses related to eye movements in awake monkeys. *Science* 171: 82–84, 1971.

Wurtz RH and Goldberg ME. Activity of superior colliculus in behaving monkey. III. Cells discharging before eye movements. *J Neurophysiol* 35: 575–586, 1972.

Wurtz RH and Mohler CW. Selection of visual targets for the initiation of saccadic eye movements. *Brain Res* 71: 209–214, 1974.

Zeki S, Watson JD, Lueck CJ, Friston KJ, Kennard C, and Frackowiak RS. A direct demonstration of functional specialization in human visual cortex. *J Neurosci* 11: 641–649, 1991.